Journal of Membrane Science 681 (2023) 121769

Contents lists available at ScienceDirect

Journal of Membrane Science

journal homepage: www.elsevier.com/locate/memsci

Partial oxidation of biomass gasification tar with oxygen transport membranes

Lev Martinez Aguilera [a], Maria Puig-Arnavat [b], Simona Ovtar [a], Jonas Gurauskis [a,1], Jesper Ahrenfeldt [b], Ulrik Birk Henriksen [b], Peter Vang Hendriksen [a], Ragnar Kiebach [a], Astri Bjørnetun Haugen [a,*]

[a] Department of Energy Conversion and Storage, Technical University of Denmark, 2800, Kgs. Lyngby, Denmark
[b] Department of Chemical and Biochemical Engineering, Technical University of Denmark, 2800, Kgs. Lyngby, Denmark

A B S T R A C T

Dual phase oxygen transport membranes were directly integrated into the producer gas stream of a low temperature circulating fluidized bed (LT-CFB) gasifier for partial oxidation of tar. $Ce_{0.9}Gd_{0.1}O_{1.95}$–$La_{0.6}Sr_{0.4}FeO_{3-d}$ composite membranes were prepared by extrusion and dip-coating, co-sintered and infiltrated with electrocatalysts. These were investigated in two different set-ups: i) a membrane test rig, and ii) a partial oxidation testing unit connected to a biomass gasifier. The stability and performance of the membrane were tested in two different gas-streams; i) H_2 and ii) producer gas. An oxygen flux of 1.5 Nml•cm^{-2}•min^{-1} was measured in an air/H_2 gradient at 850 °C through a 10 cm long membrane with a diameter of 10 mm, whereas a lower oxygen flux of 0.5 Nml•cm^{-2}•min^{-1} was measured for the air/producer gas case. The producer gas contained ca. 2000 mg Nm^{-3} of primary tar. Analysis of the gas and the tar composition at the output of the membrane unit demonstrated that it contributed to the partial oxidation of the primary tar, resulting in a twofold increase of H_2, CH_4 and CO in the producer gas. This successful integration of oxygen transport membranes demonstrated that these membranes can reduce the tar content in producer gas from biomass gasifiers.

1. Introduction

Biomass represents a renewable resource that can be used for electricity production or synthesis of green fuels. Nevertheless, it is a scare resource, the demand of which can only be expected to increase, and hence the overall efficiency of the conversion processes is important. Thermal gasification of biomass has been proven to be highly flexible and efficient if used optimally. The LT-CFB Gasification process (Fig. 1) was developed at DTU and subsequently scaled up and introduced to the market by DONG Energy (now Ørsted) under the name *Pyroneer* [1]. This gasifier was designed specifically to gasify marginal and residual biomass resources with high contents of low melting ash compounds such as straw, manure fibres, sewage sludge, organic waste etc. That have proven difficult to convert efficiently in other processes, avoiding the utilization of high quality and more costly resources such as wood. Cold gas efficiencies of 87–93% have been achieved on several feed-stocks in the LT-CFB-gasifier at DTU [1].

The process is based on separate pyrolysis- and gasification reactors with sand and ash used as an inert medium circulating through and between the reactors to transfer heat from the gasification process to the pyrolysis reactor. The maximum temperature in the char reactor (the gasification reactor) is efficiently kept below the agglomeration temperature of the circulating particles. Due to slight cooling in the pyrolysis chamber and subsequently in the primary and secondary cyclones, even alkalis that may have been partly evaporated in the hot zones are solidified before leaving the system. The alkalis can be separated together with the ash particles without including a raw gas cooler. In this way, fouling and high temperature corrosion, mainly due to condensing potassium chloride [2], can be avoided and advantageously the valuable nutrients (potassium and phosphorus) are concentrated in the ashes which are separated out. Generation of toxic PAH (Polycyclic Aromatic Hydrocarbons) compounds in the ashes is furthermore avoided, allowing their use as fertilizer and soil enhancer [3].

The commercial application of the LT-CFB platform has so far been limited to production of heat and power if the gas is fed to an adjacent power plant with a boiler and a steam cycle. The primary limiting factor for the applicability of low temperature gasification is the relatively high tar level in the producer gas [4,5].

Tar is a complex mixture of organic compounds, mostly with an aromatic structure and with a spectrum of molecular weights. According to the IEA Bioenergy, tar is defined as “all organics boiling at temperature above that of benzene” [6]. Tar originates during the pyrolysis stage

* Corresponding author.
E-mail address: ahua@dtu.dk (A.B. Haugen).
[1] Present address: ARAID at Instituto de Nanociencia y Materiales de Aragon (CSIC-Unizar), 50,018 Zaragoza, Spain.

https://doi.org/10.1016/j.memsci.2023.121769
Received 19 March 2023; Received in revised form 9 May 2023; Accepted 22 May 2023
Available online 23 May 2023

and evolves during gasification. Primary tar, mainly mixed oxygenates, are a product of pyrolysis. As gasification progresses, at higher temperatures the primary tar thermally decomposes to secondary and tertiary products and a greater quantity of light gases. The tar mixture can cause serious operational problems in downstream equipment due to high temperature condensation, leading to clogging and corrosion of components [6,7]. Thus, tar is a challenge in every biomass gasification concept. However, the concentration and composition of tars depends on the design of the gasifier and the type of biomass used as fuel. The tar composition from a low temperature gasifier operating at 800–900 °C primarily consists of phenols, with only minor amounts of PAH [8].

It is possible to remove tar using treatments inside the gasification reactor (primary methods) or in a separate downstream unit (secondary methods). Although primary methods can reduce the tar content considerably, secondary measures are generally needed to achieve complete removal. The options proposed for producer gas treatment include cold gas cleaning, hot gas filtration, thermal cracking, catalytic cracking by using metal-based or mineral catalysts. Catalytic methods are often too expensive or complex for small-scale applications where thermal methods seems more appropriate. Thermal treatment of the gas can be done either by external heating or by partial combustion of the fuel gasses [6,8]. The partial oxidation of the gas results in a significant reduction of the tar. Primary and secondary tars are oxidized or converted to tertiary tar during this partial oxidation. The efficiency of the partial oxidation of tar can be controlled by the amount of oxygen in the fuel gas, as shown by Ahrenfeldt et al. [9]. The concept of controlling the oxygen concentration, proposed in this study, is based on the integration of dense ceramic membranes in the producer gas stream. Dense ceramic membranes made from mixed oxide ionic and electronic conductive materials (MIEC) allow the separation of oxygen from the air supplied at elevated temperatures (>550 °C) [10]. The oxygen transport through the membrane occurs spontaneously via solid-state diffusion of oxide ions if the membrane is exposed to a gradient in the oxygen partial pressure, pO_2, at high temperatures. This separation process is 100% selective towards oxygen [11].

The applicability of dense oxygen transport membranes for syngas production was experimentally shown by different groups [12–15]. Furthermore, the integration of oxygen transport membranes into an experimental coal gasifier was reported by Gupta et al. [13]. The majority of the research in developing oxygen transport membranes has focused on two different groups of materials; i) acceptor doped perovskite-type oxides; $La_{1-x}A_xCo_{1-y}B_yO_{3-d}$ (A = Sr, Ba; B=Fe, Mn, Cr), and ii) acceptor doped fluorite-type oxides like $Ce_{1-x}M_xO_{2-d}$ (M = Gd, Sm, Pr) [12]. Recently, composites of those materials has attracted large interest in the oxygen transport membrane research [16–20]. Composite membranes, also called dual-phase membranes, enable an easier tuning of the required properties, especially the simultaneous maximization of both oxide-ion and electronic conductivity [21].

For the partial oxidation of tar, the membranes must be stable in a steep pO_2 gradient, with air on one side and producer gas on the other side of the membrane. Additionally, the membrane material must show the required performance in terms of oxygen flux, chemical stability and mechanical reliability.

The aim of this study is to demonstrate a proof of concept of the direct integration of an oxygen transport membrane into the producer gas stream of an LT-CFB gasifier for partial oxidation of tar. Dual-phase composite membranes based on $Ce_{0.9}Gd_{0.1}O_{1.95}$ (CGO) – $(La_{0.6}Sr_{0.4})_{0.98}FeO_{3-d}$ (LSF) were selected for the partial oxidation of tar in the producer gas. This membrane composition was chosen based on our in-house experience with this system and its previously reported promising results [17], including stability in low pO_2 over more than 900 h [22]. Previous work [22] also showed that despite these materials' mixed conduction ability, it can be approximated that at the conditions of the current study, the CGO and LSF phases are solely responsible for the ionic and electronic conductivity, respectively. A-site deficient $(La_{0.6}Sr_{0.4})_{0.98}FeO_{3-d}$ was used due to commercial availability of this composition, and since A-site deficiency gives higher stability towards the formation of hydroxides and carbonates of Sr and La, which can lead to mechanical disintegration of the sample [23]. To the best of the authors' knowledge, this is the first study that reports the direct integration of an oxygen transport membrane into a producer gas stream.

2. Materials and methods

2.1. Feedstock for gasification

The biomass used in the LT-CFB gasifier was wheat straw crushed pellets, with composition as listed in Table 1.

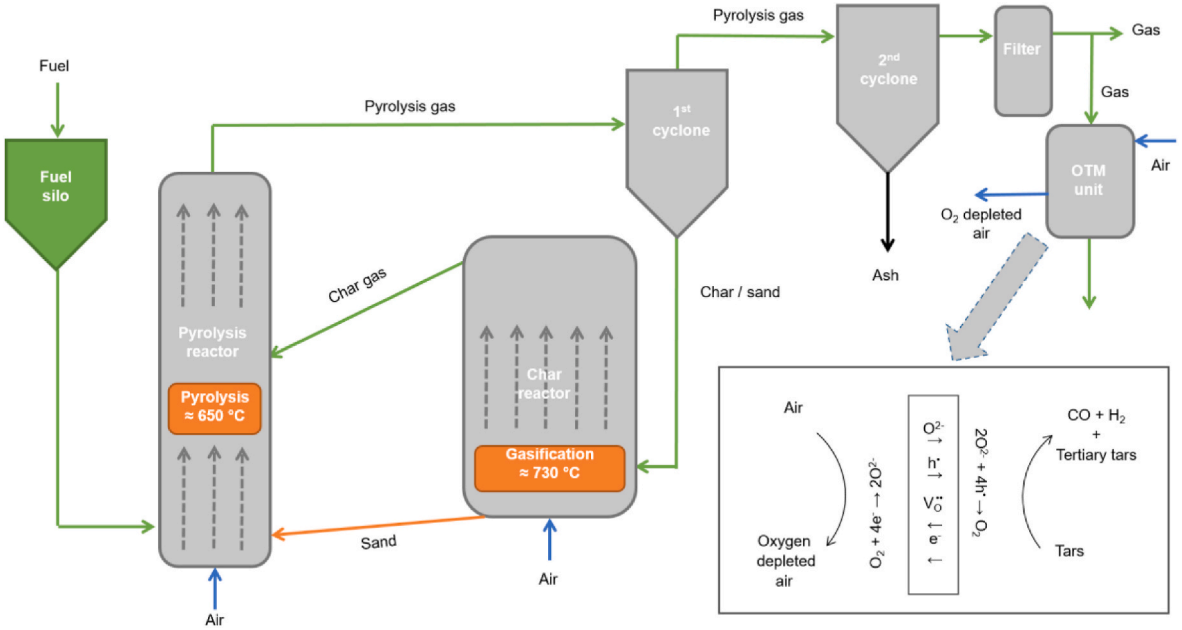

Fig. 1. LT-CFB gasifier flow diagram with the operating principle of a dense ceramic membrane for the partial oxidation of tar.

Table 1
Composition and characteristics of wheat straw crushed pellets, all weight-based (ar: as received, db: dry basis).

Proximate analysis		
Parameter	Unit	Value
Moisture content	% ar	10.6
Volatiles	% db	68.4
Fixed Carbon	% db	23.8
Ash	% db	7.8
Ultimate analysis		
Parameter	**Unit**	**Value**
Carbon (C)	% db	47.1
Nitrogen (N)	% db	0.8
Hydrogen (H)	% db	5.8
Oxygen (O)	% db	38.2
Chlorine (Cl)	% db	0.13
Sulphur (S)	% db	0.17
Elemental composition		
Aluminium (Al)	mg/kg db	150
Calcium (Ca)	mg/kg db	6080
Iron (Fe)	mg/kg db	190
Potassium (K)	mg/kg db	12,000
Magnesium (Mg)	mg/kg db	750
Sodium (Na)	mg/kg db	370
Phosphorus (P)	mg/kg db	680
Silicon (Si)	mg/kg db	5900

2.2. Fabrication of the oxygen transport membranes

A 10 cm tubular, asymmetric oxygen transport membrane was used for the partial oxidation of tar in this work. This component consists of a dual-phase $(La_{0.6}Sr_{0.4})_{0.98}FeO_{3-\delta}$ (LSF) and $Ce_{0.9}Gd_{0.1}O_{2-\delta}$ (CGO) 10 μm thin film as the active oxygen transport membrane. This layer is sandwiched between two 5–15 μm layers of porous CGO. These three thin layers were deposited on MgO support tubes by dip coating. After the firing of this four-layer structure the outer CGO layer was infiltrated with a catalyst according to a previously developed procedure described in Ref. [24]. The here used membrane was sintered for 4 h at 1250 °C, and only the outer porous layer was infiltrated with $LaCoO_{3-\delta}$ nanoparticles, whose catalytic properties are well-established [22]. The porous MgO supports were prepared by thermoplastic extrusion, based on the procedure described in Refs. [25,26]. The used MgO feedstocks for extrusion are based on MgO powders calcined at 900 °C. The mixture contained 20 vol% thermoplastic polymers, and 1 wt% Fe_2O_3 for improved sintering. The resulting support tubes had a porosity of 7% providing an overall gas permeability of 7×10^{-15} m^2. The flexural strength was ca. 40 MPa.

2.3. Experimental set-up

2.3.1. Lab-scale testing in membrane rig

Lab-scale oxygen permeation experiments were carried out using an open flow setup with supplying air at the outer side of the tube (feed side) and N_2, H_2 or simulated producer gas at the inner side (permeate side). Alumina holders were used to support the oxygen membranes and to supply a "flush" gas at the permeate side. The oxygen membranes were situated in the hot zone of a vertical tubular furnace. The temperature of the sample was monitored by placing thermocouples inside the alumina tube at the inlet and outlet of the oxygen membrane.

The oxygen membranes were sealed on the alumina support using glass (SiO_2, 67.94 wt%, Al_2O_3, 14.91 wt%, and Na_2O, 17.14 wt%). Indication of the gas tightness was obtained by considering the difference between the inlet and the outlet gas flow rate after high temperature sealing at 980 °C for 1 h. For an inlet flow rate of 500 l min^{-1} of N_2, an outlet flow rate of 500 l min^{-1} ± 3 ml min^{-1} was obtained. Additionally, the membrane was slightly pressurized with an inside overpressure corresponding to ca. 20 mm of H_2O (2×10^{-3} atm). The leak was below the measurement error on the outlet flow rate. Therefore, a leak-free membrane was assumed in the data-analysis.

The active membrane area, calculated as the area between the seals on the outer diameter of the oxygen membrane, was 5 cm^2. A constant air flow on the feed side (2.0 l min^{-1}) and a flow of different gasses (N_2, H_2, CO_2, CO, CH_4) on the permeate side (0.016–0.40 l min^{-1}) were supplied. The gas flow rate was controlled and measured using mass-flow controllers (Brooks). The pO_2 was measured for the inlet ($pO_{2(in)}$) and the outlet gas ($pO_{2(out)}$) on the permeate side of the membrane using an in-house built ZrO_2-based sensor.

The membranes were tested with three different permeate side gases, i) N_2, ii) H_2, and iii) simulated producer gas. In all cases, air was supplied on the feed side of the membrane. For testing in the N_2 stream and the simulated producer gas configurations, the oxygen permeation flux, $J(O_2)$, was calculated by Eq. (1).

$$J(O_2) = \frac{\Phi_{inlet}(pO_{2\ outlet} - pO_{2\ inlet})}{A * Ptot} \quad \text{Eq. 1}$$

φ_{inlet} is the total flow rate of gasses into the membrane and A is the active surface area of the membrane. For the N_2 configuration $pO_{2\ (outlet)}$ and $pO_{2\ (inlet)}$ are measured by partial oxygen pressures using the ZrO_2-based sensor. For the simulated producer gas configuration, the pO_2 values were calculated from the known total amount of C and H in the system, measured pO_2 and from known temperature dependent equilibrium constants for reactions described by Eqs. (2)–(4).

$$H_2 + \frac{1}{2}O_2 \leftrightarrow H_2OK = \frac{pH_2O}{pH_2 \bullet pO_2^{1/2}} \quad \text{Eq. 2}$$

$$CO + \frac{1}{2}O_2 \leftrightarrow CO_2K = \frac{pCO_2}{pCO \bullet pO_2^{1/2}} \quad \text{Eq. 3}$$

$$CH_4 + \frac{1}{2}O_2 \leftrightarrow CO + 2H_2\ K = \frac{pH_2^2 \bullet pCO}{pCH_4 \bullet pO_2^{1/2}} \quad \text{Eq. 4}$$

In the H_2 configuration, the equilibrium condition described by Eq. (2), was assumed and the oxygen permeation flux was calculated by Eq. (5).

$$J(O_2) = \frac{\Phi_{H_2O(outlet)} - \Phi_{H_2O(inlet)}}{2A} \quad \text{Eq. 5}$$

The volume flow rates of water (φ_{H2O}) were calculated from measured pO_2 and the known equilibrium constant ($K_{eq\text{-}1}$) (Eq. (2)), as described by Chatzichristodoulou et al. [27].

2.3.2. Unit for testing with gasifier

A specific open flow setup was designed to carry out tests with H_2, N_2 or producer gas from a side stream of the LT-CFB gasifier after the gas filter. The membrane was placed in the setup with the inner side as the permeate side and the outer side as a feed side. Alumina spacers pre-sealed on Kanthal® holders with glass at 850 °C were fixed with Inconel fittings to the testing setup (Fig. 2a). The glass paste was applied to the contact area and the oxygen membranes were placed between the alumina spacers (Fig. 2b-c).

The oxygen membranes were placed in the hot zone of the furnace, which was heated up to 850 °C with heating rate of 5 °C•min^{-1}. The oxygen membrane was sealed in-situ at 850 °C for 30 min under compression using 1 kg load provided by a pulley and counterweight system (Fig. 3a). The active membrane area was ca. 35 cm^2 between the seals of the 10 cm long membrane tube.

A stainless steel cylinder that included the air preheating section, as well as the fresh air inlet and oxygen depleted air outlet for the O_2 concentration measurement (Fig. 3a–d) was placed around the membrane tube. The lower part of the cylinder was open, so the rest of the oxygen-depleted air could freely leave the unit. Three gasometers were installed to measure the flow of air (IGA Type AC-5M B733), H_2/N_2 (IGA Type AC-5M B733) and oxygen-depleted air flow (Gallus 2100 TCE – G4

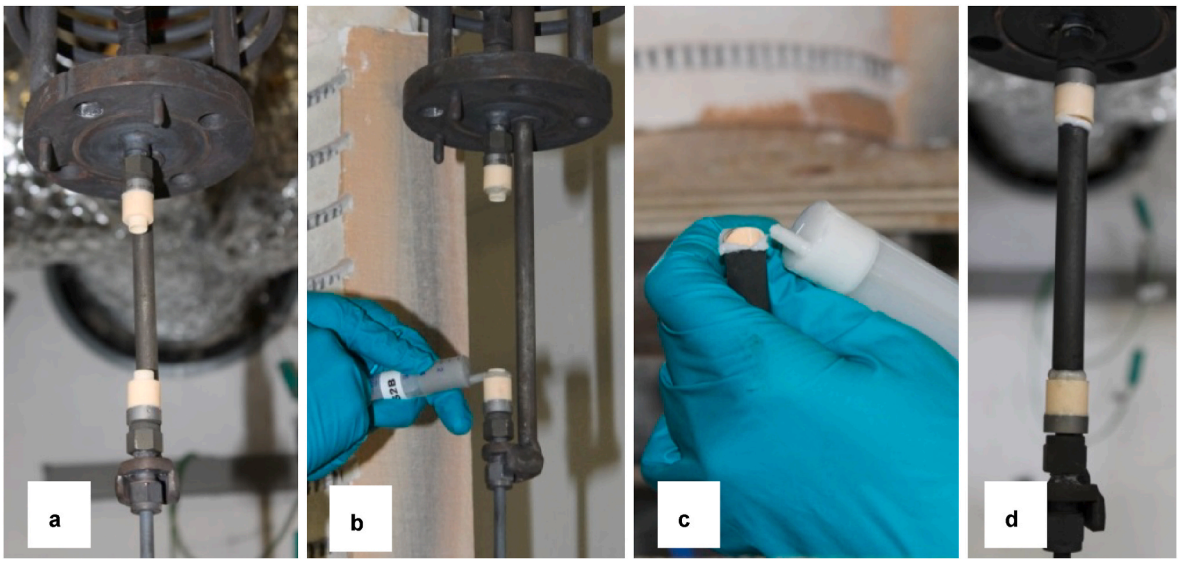

Fig. 2. Designed set-up for the oxygen membrane testing: a) alumina spacers pre-sealed on the Kanthal holder with Inconel fittings; b-c) application of the glass paste to the contact area between membranes and alumina spacers; d) oxygen membrane in place in the set-up unit.

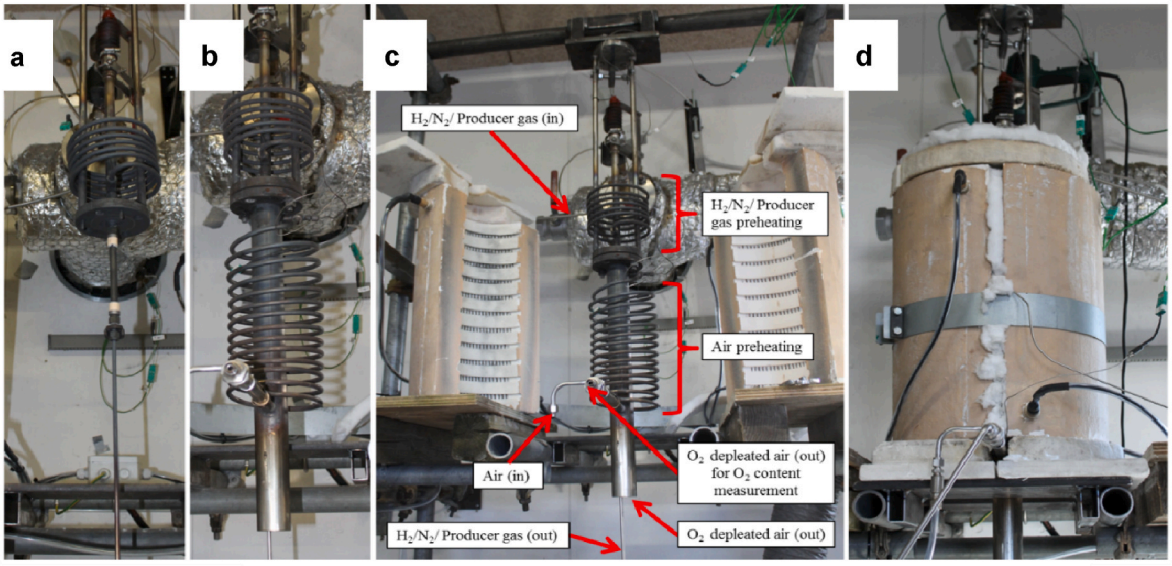

Fig. 3. Set-up for the oxygen membrane testing on a side stream of the LT-CFB gasifier: a) oxygen membrane placed in the set-up unit. Pulley and counterweight system to keep the membrane under a load is observed on the top of the unit. B) detail of the stainless steel cylinder covering the membrane with the air preheating section; c) the entire set-up placed inside the furnace; d) set-up with the furnace closed and insulated.

T) into the pO_2 sensor. These gasometers are made for the flow rate range 0.25–100 Nl•min^{-1}. Having flow rates close to the lower limit (1–3 Nl•min^{-1}) affects the accuracy of the results, however, the selection of these gasometers was based on a compromise between the accuracy of the experiments and expected operation flows in the pilot-scale gasifier. The highly accurate measurements carried out in the membrane test rig were used as reference. The system was equipped with three thermocouples to measure the inlet air temperature, the N_2/H_2/producer gas inlet temperature and the furnace temperature. Additionally, the temperature of the producer gas before and after the main valve of the side stream was measured. The connecting part between the producer gas stream and the gasifier testing unit was heated to ca. 300 °C to prevent condensation of tar.

2.3.3. Testing of membranes in N_2 and H_2

Adequacy, robustness and sensitivity of the developed partial oxidation test unit were evaluated by testing it with N_2 or H_2 as sweep gas and air as feed gas. The sealing of the membrane was done at 850 °C for 30 min while flowing air on the outside of the membrane. Afterwards, the supply tube system and the inside of the membrane were flushed with N_2 (1 l min^{-1}) for 15 min. This was followed by supplying 0.35–0.85 l min^{-1} of H_2 inside the membrane for 60 min. After this, the system was flushed with N_2 (2 l min^{-1}) again for 15 min and the membrane was passively cooled to room temperature.

During the test, pre-heated air with a flowrate of 3 l min^{-1} was supplied to the feed side of the oxygen membrane. A sample of the air (100–250 ml min^{-1}) that passed the membrane was pumped through an in-house built ZrO_2-based oxygen sensor to monitor the change of the oxygen concentration in the air feed stream.

2.3.4. Testing with producer gas

The LT-CFB gasifier was pre-warmed up for 12 h before the

combustion of fuel was started. Crushed wheat straw pellets were used as fuel and air at atmospheric pressure as gasifying agent. The oxygen membrane tests and tar measurements in the producer gas were carried out when stable operation conditions were reached ca. 4 h after the start-up. The oxygen membranes were prepared for this test following the same procedure as described for testing with N_2 and H_2. The membrane was sealed at 850 °C in air and the system was flushed with N_2 (ca. 2 l min^{-1}) for 30 min. The main valve to the side stream of the producer gas was opened and the gas flow through the membrane was monitored by measuring pressure difference before (13 mm H_2O) and after the valve (10 mm H_2O). The producer gas was pre-heated to the membrane temperature before entering the membrane. The test with producer gas was carried out over 90 min, during which the gasifier operation was stable. After the test, the main valve was closed and the system was flushed with N_2 for 15 min (ca. 2 l min^{-1}). After the test, the oxygen membrane was cooled down with a rate of ca. 7 °C•min^{-1} from 850 °C to room temperature.

Samples of the producer gas tar were taken simultaneously at the input and output streams of the partial oxidation unit for analysis. Producer gas was analysed using FLSmidth GASloq on-line gas analysers, where filters for tar-removal were set before the analysers. Additionally, gas samples for off-line analysis were taken using gas pipets attached directly to the output stream of the partial oxidation unit. Tar compositions were obtained by off-line solid phase adsorption technique (SPA) using a Hewlett Packard HP 6890 gas chromatograph interfaced to a HP5973 Mass Selective Detector (Agilent, Denmark).

2.4. Microstructural characterization of the membranes

The microstructure of the membrane before and after testing was analysed using an optical and a scanning electron microscope (SEM Merlin, Zeiss). After testing, the membrane was cut into three pieces relative to the gas flow: i) inlet, iii) middle part and iii) outlet. The polished cross sections and longitudinal sections of the membranes were prepared in an epoxy resin and their microstructure was analysed using a Hitachi TM3000 scanning electron microscope (SEM) equipped with a Bruker energy dispersive X-ray spectroscopy (EDS) system.

3. Results

3.1. Characteristics of tar and producer gas

The LT-CFB gasifier was warmed up several hours before the start up with wheat straw crushed pellets. After few hours of operation, the gasifier reached steady state of operation. This was determined from the stability of the overall mass balance and the stability of the temperature and pressure curves during operation with fixed process settings. Tar and gas compositions at the outlet of the gasifier were obtained once it reached steady state of operation, Table 2 and Table 3 show the composition of tar and the producer gas respectively.

3.2. Oxygen permeation flux measurements

Oxygen transport membranes from the same production batch were tested in two different tests units; i) a membrane test rig and ii) the gasifier test unit for producer gas. The tests that were carried out in the clean lab conditions of the membrane rig are considered highly accurate and are used as reference to evaluate and benchmark the results obtained in the gasifier test unit.

Table 3
H_2, CO/CO_2 and CH_4 content in the producer gas during stable operation of the LT-CFB gasifier.

Parameter	Results [vol%]
CH_4	3.3
CO	11.3
CO_2	19.5
H_2	3.7

In the membrane rig the membranes were tested in three different configurations, using; i) N_2, ii) H_2, and iii) simulated producer gas on the permeate site as a sweep gas. The tests in the gasifier test unit were conducted in two different configurations: i) flow of H_2 on the permeate site and ii) direct flow of the producer gas synthesized during gasification of the biomass in the LT-CFB gasifier. For all configurations, air was supplied to the feed side of the membrane.

In the following sections, the different configurations will be separately discussed and the results obtained in the membrane rig will be compared with the results obtained in the gasifier test unit.

3.3. Oxygen permeation flux in the N_2 and H_2 configurations

In Fig. 4 the oxygen permeation flux of the membrane as a function of temperature and flow rate of the sweep gas is shown. Maximum oxygen fluxes of 0.75 l/min and 6.14 l/min were measured at 850 °C using 0.4 l/min of N_2 and H_2, respectively. The oxygen permeation flux was strongly influenced by the flow rate of the sweep gasses.

This can be directly correlated with an increased driving force of oxygen transport through the membranes, due to faster dilution/consumption of the permeated oxygen. Also, the oxygen permeation flux is strongly temperature-dependent. The activation energy deduced from the measurements with a pO_2 at the outlet gas of 0.02 atm (for the N_2 configuration) was 112 kJ/mol and for the pO_2 of 10^{-18} atm (for the H_2 configuration) it was ca. 190 kJ/mol. A similar activation energy of 153 kJ/mol was reported by Cheng et al. [17] for planar asymmetric CGO-LSF composite membranes with LSC electro-catalyst on the feed side for air/He configuration. The high activation energy indicates that the oxygen transport through the membrane is most probably limited by the surface exchange.

Fig. 5a shows an overview of the oxygen flux measurement in the gasifier test unit with H_2 on the permeate side. The temperature was kept constant during the test at ca. 850 °C. A slight difference between the air and the sweep gas inlet temperature was observed (Fig. 5a). The membrane was first tested in N_2, then in H_2 and at the end of the test, the measurement in N_2 was repeated. The oxygen permeation flux in the N_2 configuration was ca. 0.5 Nml/cm^2 min for a flow of nitrogen of 1 l/min and. This flux was 2.5 times lower than expected from the measurements in the membrane rig run under similar conditions. The test in N_2 was repeated after 60 min of testing in H_2. A slight degradation of the oxygen permeation flux after testing in H_2 compared to the initial performance

Table 2
Composition of tar of producer gas during stable operation of a LT-CFB gasifier.

Primary tar [mg m^{-3}]		Secondary tar [mg m^{-3}]		PAH [mg m^{-3}]	
Phenol	821	Naphtalene	123	Acenaphthene	12
Dimethylphenol	202	Methylnaphtalene	98	Acenaphthylene	21
Cresol	547	Ethylnaphtalene	5	Fluorene	19
Ethyl-methylphenol	172	Dimethylnaphtalene	16	Anthracene	24
Ethylphenol	30	Vinylnaphtalene	3	Methylanthracene	8
Total	1772	Total	245	Pyrene	8
				Total	92

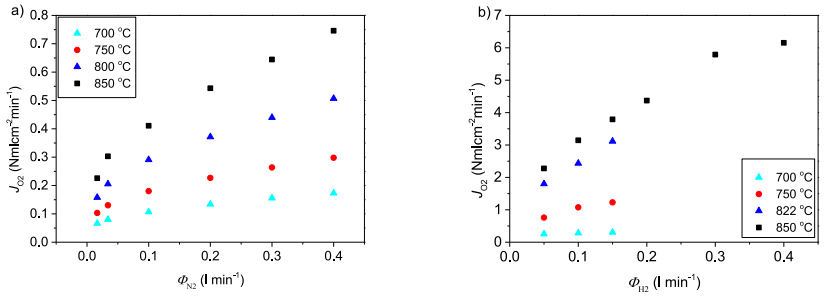

Fig. 4. Oxygen permeation flux of a $Ce_{0.9}Gd_{0.1}O_{1.95}$ – $La_{0.6}Sr_{0.4}FeO_{3-d}$ membrane (area of 5 cm^2) during lab-scale testing in membrane rig in a) nitrogen, b) hydrogen.

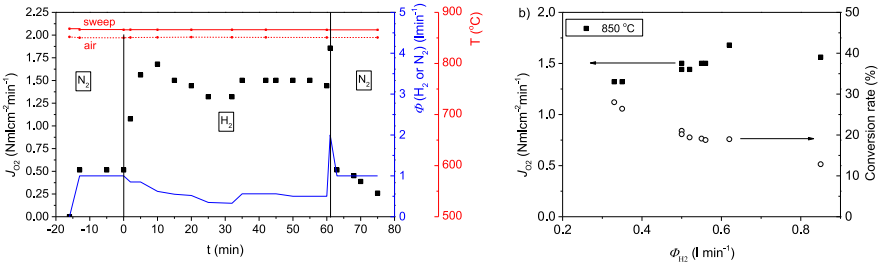

Fig. 5. a) Oxygen permeation flux $Ce_{0.9}Gd_{0.1}O_{1.95}$ – $La_{0.6}Sr_{0.4}FeO_{3-d}$ membrane (area of 35 cm^2) tested in the rig at the gasifier for a) an 80 h test with either H_2 or N_2 at the permeate side and b) oxygen permeation flux and conversion rate as a function of the hydrogen flow rate.

in N_2 was observed (Fig. 5a).

During the test in H_2 the flow rate was varied. The dependence of the oxygen permeation flux on the H_2 flow is shown in Fig. 5b. Like for the test in the membrane test rig the oxygen permeation flux increases with increased sweep flow rate. As expected, by increasing the flow rate the conversion rate was decreased. The maximal conversion rate for the 10 cm long tubular membrane was 28%. However, the flux measured in the gasifier test unit was ca. 4 times smaller than in the membrane rig for the same testing conditions (850 °C, 0.4 l/min). This difference can be ascribed to several reasons. Firstly, the driving force of the oxygen permeation is reduced along the membrane length as described by Puig-Arnavat et al., where a decrease of 13% of the oxygen flux was calculated in the first 10 cm of a MIEC tubular membrane working with air/vacuum gradient at 850 °C [15]. Therefore, for a longer membrane operating under the same conditions the total amount of oxygen permeated will be larger but the flux (transport/area) will be lower. Secondly, in the membrane rig the pressure of the gasses is slightly higher than in the gasifier test unit, which can result in different oxygen flux. Finally, the difference can also originate from a lower accuracy of the setup used at the gasifier as described below.

The oxygen permeation flux in the membrane test rig was calculated from oxygen sensor signals that accurately determine the gas-composition (hydrogen/steam-ratio) and thus effectively the flow rate of the formed water. This accurate measurement principle cannot be used in the gasifier test unit, because the tar presents in the producer gas would destroy the sensitive oxygen sensors. Instead, the flux in the gasifier membrane test unit is calculated from the depletion of oxygen on the air side. With the given flows in this configuration one determines a small change in oxygen content below 20% - the signal is proportional to the log of relative change in pO_2, which is small since the total amount of oxygen permeating through the membrane is small in comparison to the amount of oxygen fed via the air stream. If one deduces the flux from characterising the permeate side stream instead (as done in the membrane test rig) a much better accuracy is possible. For a given realistic flux and a practical feed rate the amount of oxygen in the permeate side changes much more since the amount of oxygen fed to the membrane via the N_2 stream is negligible compared to the permeating amount. For the case with hydrogen on the permeate side the oxygen sensor signal depends on the log of the ratio between the two, that will vary both as H_2 is consumed and H_2O is produced (2 mol of each for 1 mol of oxygen) by the permeating oxygen, and hence the signal varies much stronger for a given set of flux and inlet-flow values.

3.4. Testing with simulated producer gas

Fig. 6 shows the results of tests of the membranes stability in simulated producer gas. The short-term tests were performed in the membrane rig. Different gas compositions were chosen to simulate the ratio of gasses in producer gas. Two different conditions were tested: i) a gas with only H_2 and N_2 and ii) simulated producer gas with flow rate ratio of $CO:CO_2:H_2:N_2:CH_4 = 2.3:3.1:1:8.9:0.7$. In Fig. 6a a test over a duration of 50 h in the gas mixture with a N_2:H_2 flow rate ratio of 8.9:1 at 822 °C is presented. The ratio N_2 to H_2 was chosen to resemble the estimated N_2:H_2 ratio in the producer gas. An initial value of 0.86 Nml•cm^{-2}•min^{-1} and a degradation of 0.07 Nml•cm^{-2}•min^{-1} (8.1%) over the 50 h of the test were observed. Long-term stability studies of a CGO-LSF membrane on a MgO porous support in H_2 and CO_2 have been described in a previous work [22]. In that study, the CGO-LSF membrane provided an initial flux value of 1.28 Nml•cm^{-2}•min^{-1} with a degradation of 0.16 Nml•cm^{-2}•min^{-1} (12.1%) in the first 50 h of operation when working at 700 °C and flowing 200 Nml•min^{-1} of H_2 in the feed side. After that, no further degradation was observed over the 275 h of test. The initial degradation observed here is thus of similar magnitude as observed previously [22] although conditions in the two tests are not identical.

The variation of the oxygen permeation flux with the gas composition and temperature is presented in Fig. 6b. As expected, the oxygen flux at 822 °C is reduced when decreasing the concentration of H_2 in the sweep gas from 2.5 Nml•cm^{-2}•min^{-1} for a N_2:H_2 ratio of 1:1 to 0.86 Nml•cm^{-2}•min^{-1} for a N_2:H_2 ratio of 8.9:1. Lower oxygen permeation

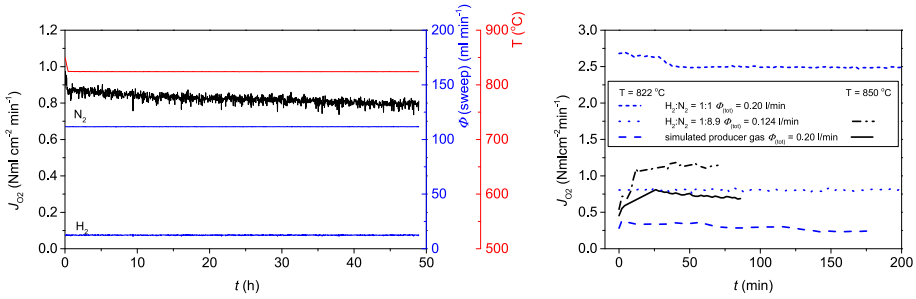

Fig. 6. Oxygen permeation flux of a CGO-LSF membrane (area 5 cm^2) in the lab-scale membrane rig as a function of time a) for a H_2:N_2 mixture of 1:8.9 at 850 °C and b) for different H_2:N_2 ratios and the simulated producer gas at 822 °C and 850 °C.

fluxes of 0.38 Nml•cm^{-2}•min^{-1} at 822 °C and ca. 0.7 Nml•cm^{-2}•min^{-1} at 850 °C were measured for the simulated producer gas, as the ratio of inert gasses (N_2, CO_2) to gasses that can react with the permeated O_2 (CO, H_2, CH_4) was increased to 3:1 and hence the driving force for the transport is reduced. The permeation flux was observed to be strongly temperature dependent. A temperature increase of 28 °C led to an increase of oxygen permeation flux of 25–50%.

3.5. Test of partial oxidation of tar

Fig. 7a shows an overview of the tests performed in the partial oxidation unit attached to the LT-CFB gasifier. The temperature of the inlet gasses was kept constant at ca. 850 °C throughout the test. The membrane was first tested in N_2, then in producer gas for ca.120 min, and finally in N_2 again to determine the degradation of the membrane. The initial performance of the membrane for a N_2 flow rate of 1.8 l min^{-1} was an oxygen flux of 0.9 Nml•cm^{-2}•min^{-1}. After the test in producer gas, the flux in N_2 had reduced to ca. 0.5 Nml•cm^{-2}•min^{-1}. These values are similar to the ones obtained in the previous tests shown in Fig. 5.

There are a several possible explanations for the lower performance of the membrane in N_2 after the short exposure to the producer gas. Degradation of perovskite-based membranes tested in CH_4 has been reported by several groups [12,28–30]. Reduced performance due to clogging of the porous MgO support with carbon due to tar decomposition is the most likely cause of degradation. It should be noted that the obtained flux values are encompassed with significant uncertainty since the gas flows are in the lower detection limits of the used gasometers and the method with quantifying the flux via the depletion of air is not very accurate.

During the test with producer gas, two different products were observed at the membrane outlet: i) condensed water and ii) white smoke, as shown in Fig. 7b. Formed water shows that partial combustion of H_2 and/or tar occurred during the test. From the observed white smoke it can be speculated that the outlet gas contained some remaining secondary and/or tertiary tars. Partial oxidation of tar in the used gasifier was studied by Ahrenfeldt et al. [1] in more detail. It was shown that a temperature of 950 °C was needed to partially oxidize primary tar, and that the predominating compound in the gas after partial oxidation was naphthalene. A detailed analysis of tar composition before and after the partial oxidation unit is shown in Fig. 8a. Phenols and naphthalenes are fully decomposed when the gas reached the outlet of the membrane, but formation of tertiary tar (PAH), such as fluorene, anthracene and pyrene were identified in the SPA analysis. This shows that a partial decomposition (and/or oxidation) of tar took place. This decomposition might be driven by the oxygen provided by the membrane, by thermal decomposition or both. In order to identify if tar conversion is thermally driven or can be ascribed to the oxygen supplied by the OTM, a 10 cm dense alumina tube, labelled “blank”, was also tested in the unit under conditions similar to the ones in the membrane test. This tube did not allow any oxygen to access the producer gas side. The results of the gas analysis for tar conversion for the “blank” are shown in Fig. 8b. Similar as when operating the membrane, phenols (primary tar) and naphthalenes (secondary tar) were fully decomposed and only tertiary tar (PAH) was observed at the outlet. This indicates that thermal decomposition played a role in the reduction of tar content in the producer gas after the membrane and the “blank”.

However, noteworthy the concentration of tertiary tar after the membrane is lower than that obtained in the alumina blank, even if the initial concentration of total phenols was higher in the membrane test. At the end of the test, tertiary tar is ca. 100 mg m^{-3} lower than those observed in the blank, considering an equivalent initial phenols concentration. When comparing the oxygen flux (Fig. 7a) and formation of tertiary tar (Fig. 8a), a correlation between the trends is observed which indicates that a fraction of the tar conversion is linked to the oxygen introduced via the membrane (the PAH content is lowest where oxygen flux is highest).

Table 4 shows the composition of the producer gas at the inlet and

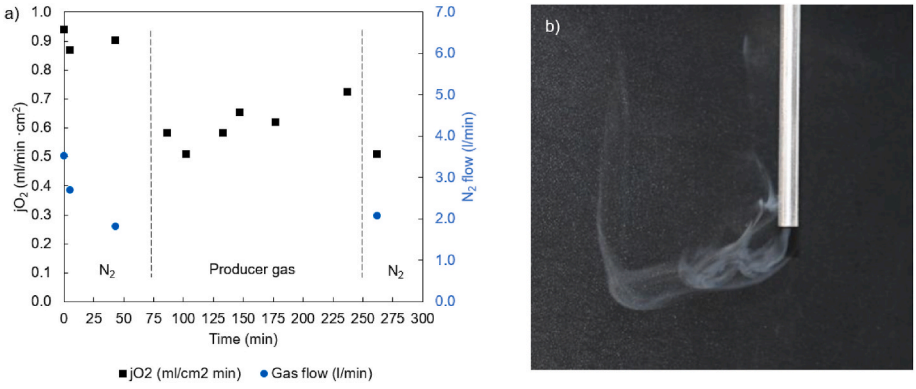

Fig. 7. a) Oxygen permeation flux of a 35 cm^2 CGO-LSF membrane tested in the partial oxidation test unit adjacent to a LT-CFB gasifier at 850 °C. b) White producer gas at the output of the membrane indicating the partial oxidation of the tar.

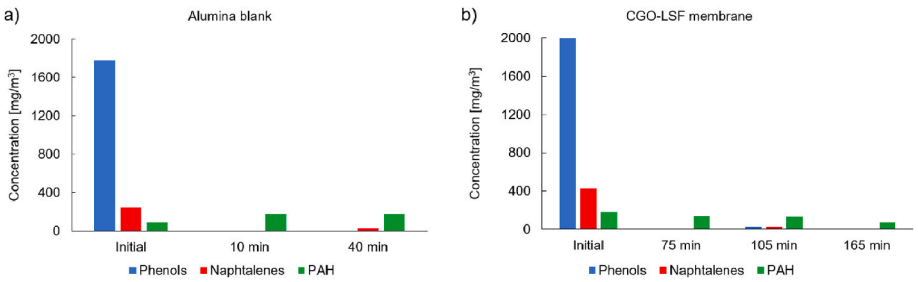

Fig. 8. Tar composition after treatment in a partial oxidation unit a) using an alumina blank and b) using a CGO-LSF membrane. Tests were carried out at 850 °C using air in the feed side. Phenols represent primary tar, naphtalenes secondary tar and PAH tertiary tar.

Table 4
Comparison of gas composition of the producer gas up and down-stream the membrane and the "blank".

Parameter	Membrane CGO-LSF			Alumina blank		
	Inlet	Membrane outlet	% change	Inlet	Blank outlet	% change
O_2	0.1	0.7	600%	0.1	0.6	500%
H_2	3.7	8.5	130%	3.7	6.6	78%
CO	12.2	12.1	−1%	13	13.4	3%
CO_2	19.5	17.4	−11%	16.9	16	−5%
CH_4	2.9	4.9	69%	3.5	5.2	49%
N_2	61.7	56.4	−9%	62.9	58.2	−7%

outlet of the partial oxidation unit when using the membrane and the alumina blank. It is noticed that the content of H_2, CH_4 and CO increases also when using an alumina blank, which shows that a purely thermal partial decomposition of tar does take place. Nevertheless, when using the membrane, ca. 50% and 20% more H_2 and CH_4 respectively are obtained than when using the blank, while the concentration of CO remains similar. Also the relative concentrations of N_2 (and CO_2) decreases stronger for the membrane case than with the blank. The decreased concentration is ascribed to the effect of a volumetric gas flow increase occurring when tar is decomposed, and hence the stronger decrease is consistent with a larger degree of tar decomposition. (The tar content at the inlet in the experiment with the blank is slightly lower than for the membrane case (1775 versus 2000 mg/m^3), however the 12% difference is too small to account for the differences reported on the outlet gas compositions between the two cases). These data, together with the direct observation of a lower concentration of tertiary tar, shows that the oxygen permeating through the membrane contributes to the tar decomposition via partial oxidation.

In the test rigs, indication of the gas tightness was obtained by considering the difference between the inlet and the outlet gas flow rate after high temperature sealing at 980 °C for 1 h. For an inlet flow rate of 500 l min-1 of N_2, an outlet flow rate of 500 l min-1 ± 3 ml min-1 was obtained, such that the leak was below the measurement error on the outlet flow rate. It was not possible to measure with the same accuracy in the gasifier setup, but since the oxygen flux values obtained in the gasifier rig were lower than those obtained in the lab rig in the same conditions, we do not have any indications of oxygen leaks from the air side into the membrane. Furthermore, if there was a considerable oxygen leak, the combination of tars and oxygen at 850 °C would mostly form CO_2 and CO; however, there was a decrement or no change in these gases when using the membrane or the alumina blank (Table 4).

3.6. Post-mortem analysis

The post-mortem analysis of the oxygen membrane tested in the partial oxidation unit is presented in Fig. 9 – Fig. 12. For the samples tested with H_2 sweep, no degradation or changes in the microstructure were observed. Fig. 9 shows a photo of a membrane after test with producer gas. The membrane was removed from the testing unit by breaking it close to the sealing area. Traces of black material were observed in the inner part of the tube in the inlet side.

Fig. 10a shows optical microscopy images of a polished longitudinal section of the membrane's porous support after testing with the producer gas. On the inlet side of the tube a residual carbon contamination (black phase) was observed with the depth of few millimetres. In the middle and on the outlet side of the tube residual carbon was not observed. It can be concluded, that the carbon was formed during the partial oxidation of methane and tar, when the concentration of permeated oxygen was not sufficient for the formation of CO and H_2.

The residual carbon in the porous support in Fig. 10a – Inlet matches with the fact that the concentration of tar is the highest at the inlet of gasses and is reduced along the tube. The main disadvantage of the carbon deposition on top the support and inside the pores is the associated clogging reducing the active area over which a partial oxidation can occur. The residual carbon is also clearly observable in Fig. 10b, where SEM micrographs of the fractured surface on the inlet side of the MgO support is shown. The clogging of the pores was almost complete at the gas inlet. The thickness of clogged area was ca. 10 μm. Below this layer the usual microstructure of the MgO support was observed.

Fig. 11 shows the polished cross section SEM micrographs of the membrane and the CGO-porous layers of different sections along the tube. EDS analysis performed on the membrane revealed that no

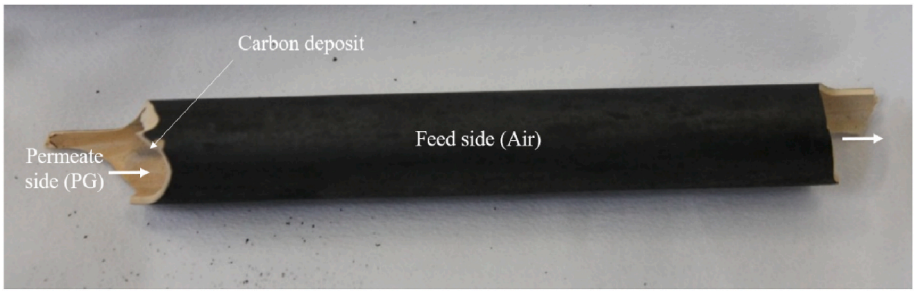

Fig. 9. Oxygen membrane after producer gas testing, showing carbon deposition (black colour) inside the tube (permeate side). (For interpretation of the references to colour in this figure legend, the reader is referred to the Web version of this article.)

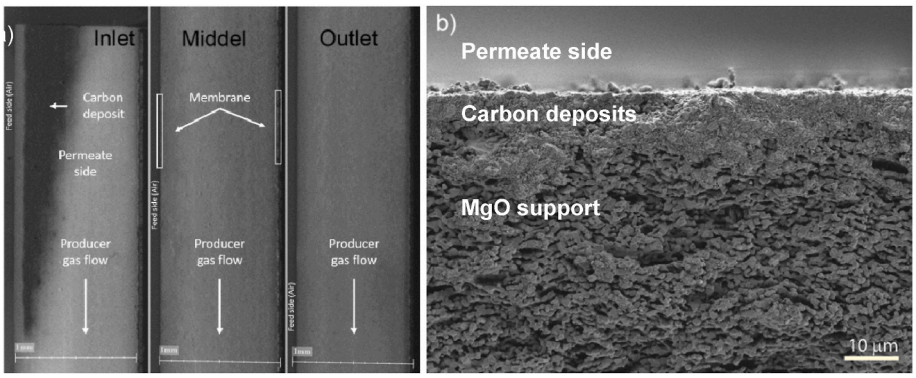

Fig. 10. Post-mortem analysis after testing in producer gas. a) Optical micrographs of the permeate side of three longitudinal sections of the OTM tube: inlet side, middle and outlet side, b) SEM micrographs of fractured cross section of the inlet side.

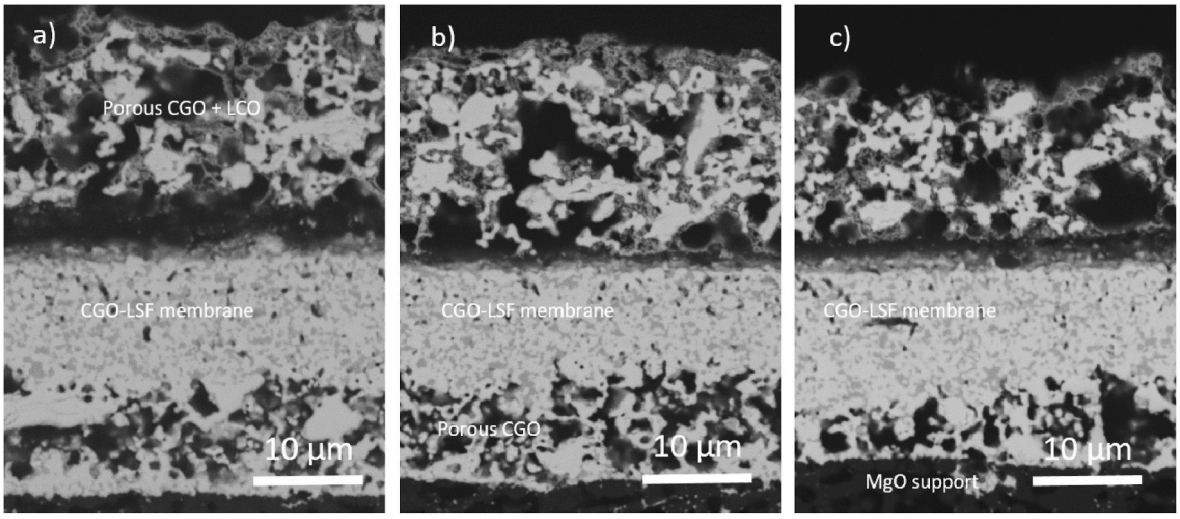

Fig. 11. Micrographs of the CGO-LSF membrane tube and the membrane layer after testing in the gasifier test unit with the producer gas of a) inlet, b) middle, c) outlet.

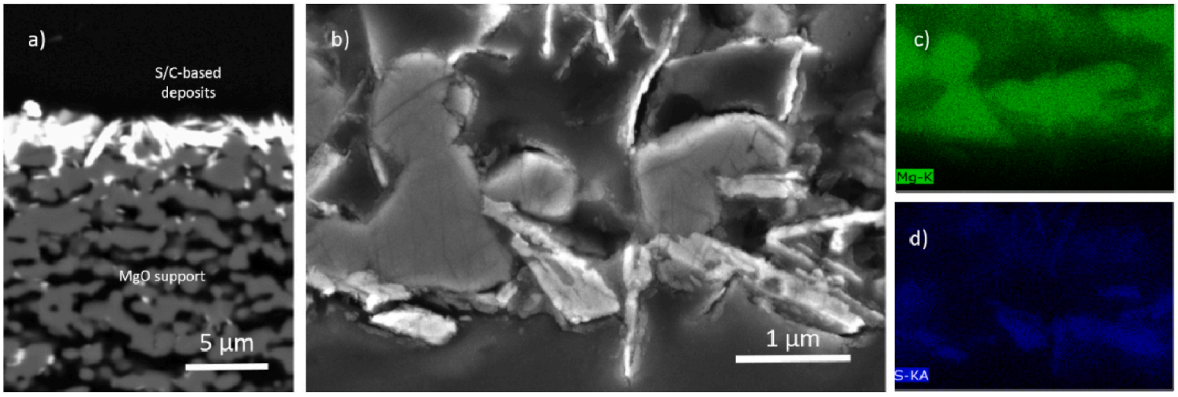

Fig. 12. a/b) Micrographs of post-mortem samples showing needle-alike structures on the permeate side of the MgO support. c/d) EDS mapping of the needles and nearby components.

additional elements are present in the feed side and no visible degradation was observed. In addition, the membrane layer is well attached to the MgO porous support, and the electro-catalyst infiltrated into the outer porous CGO layer did not coarse during testing. We can therefore conclude that there is no chemical degradation of the active membrane materials during the partial oxidation of tars in the biomass gasifier, either due to interactions with the environment or the other components of the multi-layered tube, like the MgO substrate.

Fig. 12 shows a micrograph of the permeate side of the MgO support in Fig. 10b after polishing. It is observed that needle-like structures are formed on the surface of the MgO support. A higher resolution micrograph (Fig. 12b) as well as its EDS mapping (Fig. 12c and d) shows that the deposits are not only composed of C, C_xH_y or tar, but also contain sulphur. These compounds were not observed within the MgO support,

but only on surface of the permeate side (producer gas side). Although the random distribution of these compounds do not affect the diffusion of the gases throughout the porous support, it is likely that during long-term operation they could negatively affect the performance of the membrane.

One important improvement needed for further developed membranes is their mechanical robustness towards reducing conditions and thermal cycling. After testing, attempts to cool down and heat up again the membrane led to severe delamination between the membrane layer and the support. The delamination might in principle occur due to thermal expansion coefficient (TEC) mismatch of the materials [19]. However, the here pursued material combination is overall fairly well matched; MgO has a TEC of 15.6 × 10^{-6} K^{-1} (30–1000 °C) and 14.4 × 10^{-6} K^{-1} (30–850 °C) [31], LSF doped with 40% Sr has a TEC of 17.9 × 10^{-6} K^{-1} (30–1000 °C) [32] and the CGO of 12.72 × 10^{-6} K^{-1} (30–850) [33]. However, importantly at temperatures higher than 600 °C in reducing conditions, an expansion of the CGO lattice occurs, causing a chemical (or "stoichiometric") expansion [34]. Also the LSF will expand on reduction [35]. These expansions will create mechanical stresses in the four layer structure that may cause a delamination between the membrane layer and the porous CGO layer or between the support and the CGO layer. Mechanical failure of membranes due to these effects have previously been reported and discussed in several papers [14,35,36].

The results in the tests with producer gas demonstrates that the tested membranes are capable of oxidizing the tar and generate "permanent gases". The observed carbon deposition issue would likely be alleviated by; 1) operating with a more moist gas, 2) operating with a membrane providing locally a higher oxygen flux, and finally 3) with modified designs, where there is not a thick porous inert medium (like MgO) between the electrocatalytically active CGO in the membrane and catalyst layer and the gas-stream. Further work is needed to clarify if these suggestions could eliminate the carbon formation issue. Also for the membranes here tested the delamination of the layers limit the use of the membranes in practical applications, as the pieces are not sufficiently robust to thermal cycling after use. Thus, development of chemically stable and mechanically more robust oxygen transport membranes is required to benefit from their integration in biomass gasification.

4. Conclusions

Tubular oxygen transport membranes based on dense composite $Ce_{0.9}Gd_{0.1}O_{1.95}$ – $La_{0.6}Sr_{0.4}FeO_{3-d}$ (CGO-LSF) layers supported on porous MgO were successfully integrated and tested in a biomass gasification unit for the first time. The partial oxidation of tar in the producer gas of a low temperature continuous fluidized bed (LT-CFB) gasifier was investigated in a specially designed testing unit. The combination of heat and oxygen provided by the membrane process led to a 65% reduction in tertiary tar, and an additional 50% and 20% higher conversion of the tar into H_2 and CH_4 when comparing with the purely thermal conversion of these tars.

The oxygen flux through the 10 cm long membrane placed in an air/H_2 gradient at 850 °C measured in the gasifier unit was 1.5 Nml•cm^{-2}•min^{-1}, which corresponded to ca. 30% conversion of the H_2 fed to the membrane. The short-term stability of the CGO-LSF membrane operating at 850 °C between air and producer gas was successfully demonstrated. In addition to the tests in the biomass gasifier, the performance of the membranes in H_2 and simulated producer gas were investigated under clean laboratory conditions. Here, maximum oxygen fluxes of 0.7 Nml•cm^{-2}•min^{-1} and 4.4 Nml•cm^{-2}•min^{-1} were measured at 850 °C using 0.2 l/min of simulated producer gas and H_2, respectively.

Post-mortem analysis of the membranes revealed that the performance decrease after exposure to the producer gas is most likely related to the deposition of carbon and sulphur-based compounds in the porous MgO support in the inlet area of the membrane tube. The use of an oxygen membrane for partial oxidation of the tar in producer gas was thus demonstrated. The type of membrane used, though providing decent fluxes and processing the required chemical stability for the application, needs to be improved with respect to mechanical robustness for practical application, as it does not survive thermal cycling after the test.

Author statement

LMA: investigation, methodology, writing- original draft. MP-A: investigation, methodology, writing - review and editing. SO: investigation, methodology, writing - original draft. JG: resources. JA: conceptualization, methodology. UBH: conceptualization, methodology. PVH: conceptualization, methodology, writing - review and editing. RK: conceptualization, methodology, writing - review and editing. ABH: conceptualization, methodology, resources, writing - review and editing.

Declaration of competing interest

The authors declare that they have no known competing financial interests or personal relationships that could have appeared to influence the work reported in this paper.

Data availability

Data will be made available on request.

Acknowledgments

This project has received funding from the European Union's Horizon 2020 research and innovation programme under grant agreement no.101022432 (FLEXSNG project) and from "Highly Flexible Energy Production by Oxy-Fired Biomass Gasification (HighFlex)" EUDP grant No.: 64018–0028 (previously 12403).

References

[1] J. Ahrenfeldt, T.P. Thomsen, U. Henriksen, L.R. Clausen, Biomass gasification cogeneration – a review of state of the art technology and near future perspectives, Appl. Therm. Eng. 50 (2013) 1407–1417, https://doi.org/10.1016/j.applthermaleng.2011.12.040.
[2] T. Yang, K. Jia, X. Kai, Y. Sun, Y. Li, R. Li, A study on the migration behavior of K, Na, and Cl during biomass gasification, Bioresources 11 (2016) 7133–7144.
[3] H. Hvidtfeldt, S. Petersen, DTU International Energy Report 2012: energy efficiency improvements: a key element in the global transition to non-fossil energy, Tech. Univ. Den. 1 (2012) 1–159. https://orbit.dtu.dk/en/publications/dtu-international-energy-report-2012-energy-efficiency-improvemen.
[4] S.K. Sansaniwal, M.A. Rosen, S.K. Tyagi, Global challenges in the sustainable development of biomass gasification: an overview, Renew. Sustain. Energy Rev. 80 (2017) 23–43, https://doi.org/10.1016/J.RSER.2017.05.215.
[5] J.A. Ruiz, M.C. Juárez, M.P. Morales, P. Muñoz, M.A. Mendívil, Biomass gasification for electricity generation: review of current technology barriers, Renew. Sustain. Energy Rev. 18 (2013) 174–183, https://doi.org/10.1016/J.RSER.2012.10.021.
[6] T.A. Milne, R.J. Evans, N. Abatzoglou, Biomass gasifier "tars": their nature, formation, and conversion, Nat. Renew. Energy Lab. 1 (1998), 1-204 NREL/TP-570-25357, https://www.nrel.gov/docs/fy99osti/25357.pdf, 1-204 NREL/TP-570-25357.
[7] G. Ravenni, Application of biomass char to tar conversion and producer gas upgrading to syngas, PhD thesis, Tech. Univ. Den 1 (2018) 1–239, https://orbit.dtu.dk/en/publications/application-of-biomass-char-to-tar-conversion-and-producer-gas-up.
[8] J. Fjellerup, J. Ahrenfeldt, U. Henriksen, B. Gøbel, Formation, decomposition and cracking of biomass tars in gasification, Tech. Univ. Den. (2005), 87-7475-326-6, https://orbit.dtu.dk/en/publications/formation-decomposition-and-cracking-of-biomass-tars-in-gasificat.
[9] J. Ahrenfeldt, H. Egsgaard, W. Stelte, T. Thomsen, U.B. Henriksen, The influence of partial oxidation mechanisms on tar destruction in TwoStage biomass gasification, Fuel 112 (2013) 662–680, https://doi.org/10.1016/j.fuel.2012.09.048.
[10] Y. Wei, W. Yang, J. Caro, H. Wang, Dense ceramic oxygen permeable membranes and catalytic membrane reactors, Chem. Eng. J. 220 (2013) 185–203, https://doi.org/10.1016/j.cej.2013.01.048.

[11] M.J. Den Exter, W.G. Haije, J.F. Vente, Viability of ITM technology for oxygen production and oxidation processes: material, system, and process aspects, Inorg. Membr. Energy Environ. Appl. (2009) 27–51, https://doi.org/10.1007/978-0-387-34526-0_2.
[12] H.J.M. Bouwmeester, Dense ceramic membranes for methane conversion, Catal. Today (2003) 141–150, https://doi.org/10.1016/S0920-5861(03)00222-0.
[13] S. Gupta, J.J. Adams, J.R. Wilson, E.G. Eddings, M.K. Mahapatra, P. Singh, Performance and post-test characterization of an OTM system in an experimental coal gasifier, Appl. Energy 165 (2016) 72–80, https://doi.org/10.1016/j.apenergy.2015.12.077.
[14] A. Kaiser, S. Foghmoes, C. Chatzichristodoulou, M. Søgaard, J.A. Glasscock, H. L. Frandsen, P.V. Hendriksen, Evaluation of thin film ceria membranes for syngas membrane reactors—preparation, characterization and testing, J. Membr. Sci. 378 (2011) 51–60, https://doi.org/10.1016/j.memsci.2010.12.012.
[15] M. Puig-Arnavat, S. Soprani, M. Søgaard, K. Engelbrecht, J. Ahrenfeldt, U. B. Henriksen, P.V. Hendriksen, Integration of mixed conducting membranes in an oxygen–steam biomass gasification process, RSC Adv. 3 (2013), 20843, https://doi.org/10.1039/c3ra44509g.
[16] R. Yuan, W. He, Y. Zhang, J.-F. Gao, C. Chen, Preparation and characterization of supported planar $Zr_{0.84}Y_{0.16}O_{1.92}$-$La_{0.8}Sr_{0.2}Cr_{0.5}Fe_{0.5}O_{3-\delta}$ composite membrane, J. Membr. Sci. 499 (2016) 335–342, https://doi.org/10.1016/j.memsci.2015.10.066.
[17] S. Cheng, H. Huang, S. Ovtar, S.B. Simonsen, M. Chen, W. Zhang, M. Søgaard, A. Kaiser, P.V. Hendriksen, C. Chen, High-performance microchanneled asymmetric $Gd_{0.1}Ce_{0.9}O_{1.95-\delta}$ –$La_{0.6}Sr_{0.4}FeO_{3-\delta}$-based membranes for oxygen separation, ACS Appl. Mater. Interfaces (2016) 5b10714, https://doi.org/10.1021/acsami.5b10714, acsami.
[18] J. Garcia-Fayos, V.B. Vert, M. Balaguer, C. Solís, C. Gaudillere, J.M. Serra, Oxygen transport membranes in a biomass/coal combined strategy for reducing CO_2 emissions: permeation study of selected membranes under different CO_2-rich atmospheres, Catal. Today 257 (2015) 221–228, https://doi.org/10.1016/J.CATTOD.2015.04.019.
[19] A.B. Haugen, L.M. Aguilera, K. Kwok, T. Molla, K.B. Andersen, A. Kaiser, P. V. Hendriksen, R. Kiebach, Exploring the processing of tubular chromite- and zirconia-based oxygen transport membranes, Ceramics 1 (2018) 229–245, https://doi.org/10.3390/ceramics1020019.
[20] L.M. Aguilera, S. Pirou, P. Khajavi, J. García-Fayos, J.M. Serra, H.L. Frandsen, P. V. Hendriksen, A. Kaiser, R. Kiebach, A.B. Haugen, Stable, asymmetric, tubular oxygen transport membranes of $(Sc_2O_3)_{0.10}(Y_2O_3)_{0.01}(ZrO_2)_{0.89}$ – $LaCr_{0.85}Cu_{0.10}Ni_{0.05}O_{3-\delta}$, Open Ceram. 11 (2022) https://doi.org/10.1016/J.OCERAM.2022.100292.
[21] R. Kiebach, S. Pirou, L. Martinez Aguilera, A.B. Haugen, A. Kaiser, P.V. Hendriksen, M. Balaguer, J. García-Fayos, J.M. Serra, F. Schulze-Küppers, M. Christie, L. Fischer, W.A. Meulenberg, S. Baumann, A review on dual-phase oxygen transport membranes: from fundamentals to commercial deployment, J. Mater. Chem. A. 10 (2022) 2152–2195, https://doi.org/10.1039/D1TA07898D.
[22] S. Ovtar, J. Gurauskis, A.B. Haugen, C. Chatzichristodoulou, A. Kaiser, P. V. Hendriksen, Oxygen transport properties of tubular $Ce_{0.9}Gd_{0.1}O_{1.95}$-$La_{0.6}Sr_{0.4}FeO_{3-d}$ composite asymmetric oxygen permeation membranes supported on magnesium oxide, J. Membr. Sci. 523 (2017) 576–587, https://doi.org/10.1016/j.memsci.2016.09.060.
[23] D. Tripković, R. Küngas, M.B. Mogensen, P.V. Hendriksen, Surface recrystallization – an underestimated phenomenon affecting oxygen exchange activity, J. Mater. Chem. A. 7 (2019) 11782–11791, https://doi.org/10.1039/C9TA02607J.
[24] J. Gurauskis, S. Ovtar, A. Kaiser, M. Sogaard, P.V. Hendriksen, Ceria based composite membranes for oxygen separation, ECS Trans. 64 (2014) 251–258, https://doi.org/10.1149/06402.0251ecst.
[25] D.K. Ramachandran, F. Clemens, A.J. Glasscock, M. Søgaard, A. Kaiser, Tailoring the microstructure of porous MgO supports for asymmetric oxygen separation membranes: optimization of thermoplastic feedstock systems, Ceram. Int. (2014), https://doi.org/10.1016/j.ceramint.2014.03.017.
[26] A.B. Haugen, A. Geffroy, A. Kaiser, V. Gil, MgO as a non-pyrolyzable pore former in porous membrane supports, J. Eur. Ceram. Soc. 38 (2018) 3279–3285, https://doi.org/10.1016/j.jeurceramsoc.2018.02.039.
[27] C. Chatzichristodoulou, M. Søgaard, J.a. Glasscock, A. Kaiser, S.P.V. Foghmoes, P. V. Hendriksen, Oxygen permeation in thin, dense $Ce_{0.9}Gd_{0.1}O_{1.95-\delta}$ membranes II. Experimental determination, J. Electrochem. Soc. 158 (2011) F73, https://doi.org/10.1149/1.3559189. –F83.
[28] M. Trunec, J. Cihlar, S. Diethelm, J. Herle, Tubular $La_{0.7}Ca_{0.3}Fe_{0.85}Co_{0.15}O_{3-\delta}$ perovskite membranes, Part I: preparation and properties, J. Am. Ceram. Soc. 89 (2006) 949–954, https://doi.org/10.1111/j.1551-2916.2005.00812.x.
[29] X. Zhu, W. Yang, Composite membrane based on ionic conductor and mixed conductor for oxygen permeation, AIChE J. 54 (2008) 665–672, https://doi.org/10.1002/aic.11410.
[30] M. Martin, Materials in thermodynamic potential gradients, J. Chem. Thermodyn. 35 (2003) 1291–1308, https://doi.org/10.1016/S0021-9614(03)00094-6.
[31] A.S.M. Rao, K. Narender, Studies on thermophysical properties of CaO and MgO by γ -ray attenuation, J. Thermodyn. 2014 (2014), https://doi.org/10.1155/2014/123478.
[32] K.K. Hansen, Evaluation of LSF based SOFC cathodes using cone-shaped electrodes and EIS, Solid State Ionics 344 (2020), 115096, https://doi.org/10.1016/J.SSI.2019.115096.
[33] H. Hayashi, M. Kanoh, C.J. Quan, H. Inaba, S. Wang, M. Dokiya, H. Tagawa, Thermal expansion of Gd-doped ceria and reduced ceria, Solid State Ionics 132 (2000) 227–233, https://doi.org/10.1016/S0167-2738(00)00646-9.
[34] S.R. Bishop, D. Marrocchelli, C. Chatzichristodoulou, N.H. Perry, M.B. Mogensen, H.L. Tuller, E.D. Wachsman, Chemical expansion: implications for electrochemical energy storage and conversion devices, Annu. Rev. Mater. Res. 44 (2014) 205–239, https://doi.org/10.1146/ANNUREV-MATSCI-070813-113329.
[35] M. Søgaard, P. Vang Hendriksen, M. Mogensen, Oxygen nonstoichiometry and transport properties of strontium substituted lanthanum ferrite, J. Solid State Chem. 180 (2007) 1489–1503, https://doi.org/10.1016/J.JSSC.2007.02.012.
[36] P.V. Hendriksen, P.H. Larsen, M. Mogensen, F.W. Poulsen, K. Wiik, Prospects and problems of dense oxygen permeable membranes, Catal. Today 56 (2000) 283–295, https://doi.org/10.1016/S0920-5861(99)00286-2.